

We are IntechOpen, the world's leading publisher of Open Access books Built by scientists, for scientists

6,100

Open access books available

149,000

International authors and editors

185M

Downloads

Our authors are among the

154

Countries delivered to

TOP 1%

most cited scientists

12.2%

Contributors from top 500 universities



WEB OF SCIENCE™

Selection of our books indexed in the Book Citation Index
in Web of Science™ Core Collection (BKCI)

Interested in publishing with us?
Contact book.department@intechopen.com

Numbers displayed above are based on latest data collected.
For more information visit www.intechopen.com



A Mapping Relationship-Based near-Field Acoustic Holography

Haijun Wu and Weikang Jiang

Abstract

A mapping relationship-based near-field acoustic holography (MRS-based NAH) is a kind of innovative NAH by exploring the mapping relationship between modes on surfaces of the boundary and hologram. Thus, reconstruction is converted to obtain the coefficients of participant modes on holograms. The MRS-based NAH supplies an analytical method to determine the number of adopted fundamental solution (FS) as well as a technique to approximate a specific degree of mode on patches by a set of locally orthogonal patterns explored for three widely used holograms, such as planar, cylindrical, and spherical holograms. The NAH framework provides a new insight to the reconstruction procedure based on the FS in spherical coordinates. Reconstruction accuracy based on two types of errors, the truncation errors due to the limited number of participant modes and the inevitable measurement errors caused by uncertainties in the experiment, are available in the NAH. An approach is developed to estimate the lower and upper bounds of the relative error. It supplies a tool to predict the error for a reconstruction under the condition that the truncation error ratio and the signal-to-noise ratio are given. The condition number of the inverse operator is investigated to measure the sensitivity of the reconstruction to the input errors.

Keywords: near-field acoustic holography, mapping relationship, integral identity, acoustic measurement, spherical fundamental solutions

1. Introduction

To locate the position and target the strength of noise for a vibrating structure, near-field acoustic holography (NAH) had been widely adopted as an effective tool. It has a significant influence on the noise diagnostics, which gives a permission to get all desired acoustic quantities, such as pressure, particle velocity, and sound power, from a number of discrete field measurement.

It was originally developed by Williams, Manynard, etc., to reconstruct surface velocity of a rectangular plane with Fourier transform technique [1–3]. Initially, the Fourier-based NAH decomposes the field pressure into k-space (wave number space) for baffled problems. In other words, the field pressure is expanded into plane waves, and the reconstruction procedure is to obtain coefficients of the plane waves based on measured pressure. Although different from the k-space decomposition, concept of

Fourier transformation was inherent to the 3D cylindrical and spherical NAH problems as the in-depth discussions in Ref. [4].

Since it was proposed [1], varieties of approaches had been proposed and their superiorities had been proven in various applications, which resulted in several categories according to their underlying theories. Statistical optimal NAH [5–7] uses the elemental waves to approach the acoustic field, in which the surface-to-surface projection of the sound field is performed by using a transfer matrix defined in such a way that all propagating waves and a weighted set of evanescent waves are projected with optimal average accuracy [6]. Boundary element method (BEM)-based NAH [8–13] is appropriate for arbitrarily shaped model in which a general transfer matrix between the surfaces of structure and hologram is derived from the integral equation. Among the BEM-based NAH, two types of integration equation are adopted: the directive formulation (Helmholtz integral equation) and indirect formulation (single- or double-layer integral equation). The quantities reconstructed by the NAH derived from directive formulation have clear physical meaning [8–10], while the ones obtained by NAH derived from the indirect formulation are not the real physical quantities [11–13]. The equivalent source method (ESM) [14–19], also named as wave superposition algorithm (WSA) [16, 20, 21], was proposed by Koopman [22] for solving acoustic radiation problems of closed sources. ESM assumes that the field is generated by a series of simple sources such as monopoles and dipoles, and numerical integration is not needed in determining the source strength for a set of prescribed positions. Despite versatility of the ESM and various successful applications, “retreat distance” between the actual source surface and the virtual source cannot be well defined and deserves more attention in the application [23]. The Helmholtz equation least square method (HELs) [24–26] adopted the spherical wave expansion theory to reconstruct acoustic pressure field from a vibrating structure. Coefficients of the spherical wave function, the fundamental solution (FS) for the Helmholtz equation, are determined by requiring the assumed form of solution to satisfy the pressure boundary condition at the measurement points. Since the spherical wave functions solve the Helmholtz equation directly, it is immune to the nonuniqueness difficulty inherent in BEM-based NAH [27]. However, HELs works better for spherical or chunky model than elongated model due to the specific basis function [25].

Essentially speaking, NAH is to achieve the desired acoustic quantities by the measured physical quantities such as sound pressure in the field. Most of the methods explicitly require the transfer operator $T(\mathbf{y}, \mathbf{x})$ between desired acoustic quantities $f(\mathbf{y})$ and measured physical quantities $\bar{p}(\mathbf{x})$. They built a linear system of $f(\mathbf{y}) = \text{inv}(T(\mathbf{y}, \mathbf{x}))\bar{p}(\mathbf{x})$ in which $\text{inv}(\star)$ represents an inverse operator, by either a general numerical method (BEM-based NAH) [8–13], or specific basis spaces such as a general Fourier basis (Fourier-based NAH) [1–4], simplified monopoles, dipoles (ESM and WSA) [14–16, 18, 20, 21], and fundamental solutions (HELs) [24–27]. The reconstruction procedure is therefore to solve the linear system to obtain the physical quantities on the boundary, such as pressure or normal velocity in BEM-based NAH, the source strength of equivalent source in ESM, coefficients of basis functions in Fourier-based NAH and HELs, and following by an extrapolation process to achieve desired acoustic quantities.

Unfortunately, all the proposed methods are very sensitive to errors which may cause reconstruction to fail. It is primarily due to abundant adoption of basis functions in the transfer operator which amplifies the errors in the inverse process. That is the reason why there have been numerous studies focusing on the development of

regularization methods to stabilize this inverse problem, such as truncated singular value decomposition [28] and the Tikhonov regularization [29]. Thus, construction of transfer operator is not a trivial process but is crucial to the feasibility and accuracy of the NAH. Concerning the theory development and practical measurement, it naturally arises a question whether there exists a guideline to determine the number and location of generalized basis function as well as measurement to obtain their coefficients for a given shape of source surface and prescribed tolerance.

The number of FS as well as number and position of the microphones array in the measurement are not well studied for the category of NAH based on the FS. Thus, one advantage of the mapping relationship-based NAH (MRS-based NAH) is the available guideline to the determination of the number of FS and measurement configuration in the FS-based NAH by exploring the mapping relationship between the modes in FS between surface and hologram, and investigating approximation of the modes with a set of locally orthogonal patterns.

As errors are inevitable in the practical measurement, it is curious to know how the errors go through the inverse operation and what influence imposed on the accuracy of the reconstruction results. To the best knowledge of authors, few works are devoted to the errors analysis of the NAH by comparing with that for the regularization methods. It is because that the NAH was usually viewed as a very ill-posed inverse problem for which regularized solution is the primary task. Thus, it is difficult to predict or estimate the reconstruction accuracy. Instead of a predictable way, numerical simulation and experimental validation are two frequently adopted methods to investigate the performance of NAH for different parameters [19, 30, 31]. For practical problems, it is hard to estimate the accuracy of the reconstructed results. Thus, one merit of our approach is the availability for predicting the reconstructed accuracy for a specific setup of the MRS-based NAH.

2. The mapping relationship-based NAH

2.1 Theorem development

As shown in **Figure 1**, assume that the fluid is homogenous, inviscid, and compressible and only undergoes small translation movement. The time harmonic sound pressure radiated from a vibrating structure into an infinite domain Ω is described by the well-known Helmholtz equation:

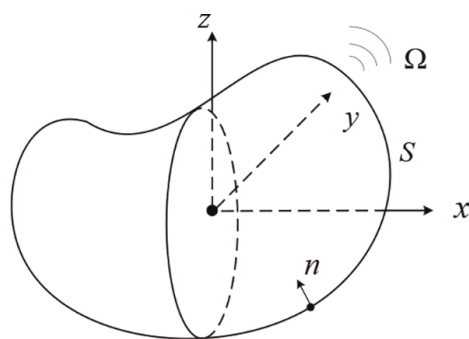


Figure 1.
Exterior acoustic problem of a vibrating structure in free space.

$$\nabla^2 p(\mathbf{x}) + k^2 p(\mathbf{x}) = 0 \text{ for } \mathbf{x} \in \Omega \quad (1)$$

where k is the wave number, relating to the acoustic speed c and angular frequency ω by $k = \omega/c$, and \mathbf{x} is a point in the domain. The time component is assumed to be $e^{-i\omega t}$.

The fundamental solution of the governing formulation Eq. (1) in the spherical coordinates is

$$S_n^m(k, \mathbf{x}) = h_n(k\|\mathbf{x}\|)Y_n^m(\theta, \phi), |m| \leq n, n = 0, 1, 2, \dots, N \quad (2)$$

where variables θ and ϕ are the polar angles of a point in the spherical coordinates and N is the truncated degree in a series expansion. j_n and h_n are the n th spherical Bessel function and spherical Hankel of the first kind, respectively. Y_n^m is the normalized spherical harmonic function:

$$Y_n^m(\theta, \phi) = \frac{1}{\sqrt{2\pi}} \bar{P}_n^m(\cos \theta) e^{im\phi} \quad (3)$$

where \bar{P}_n^m is the normalized associated Legendre function [32].

Normal gradient in the direction $n(\mathbf{x})$ for the fundamental solution Eq. (3) is as follows:

$$q_n^m(\mathbf{x}) = \frac{\partial S_n^m(\mathbf{x})}{\partial n(\mathbf{x})} = \frac{\partial h_n(k\|\mathbf{x}\|)Y_n^m(\theta, \phi)}{\partial n(\mathbf{x})} \quad (4)$$

which is related to the normal velocity v_n by the Euler formulation:

$$q(\mathbf{x}) = ik\rho c v_n(\mathbf{x}) \quad (5)$$

It should be noted that Eqs. (2) and (5) are related as a solution pair for exterior acoustic problems, which means giving one as the boundary condition, the other will be the solution. They form a set of pressure/velocity modes on the boundary of a vibrating structure, which are generally independent on nonspherical surfaces and orthogonal on spherical surfaces. To facilitate derivations, we refer the velocity modes as the normal gradient q instead of the normal velocity v_n . Assume that a structure is vibrating in one of its velocity modes Eq. (5), and the radiated pressure must be in the form of Eq. (2), which can be derived by making use of the equivalent source method (ESM) and boundary integral equation (BIE) [33].

Based on the model decomposition theorem and the mapping relationship, the boundary velocity $v(\mathbf{y})$ and the radiated sound pressure $p(\mathbf{x})$ on the hologram can be expressed for a given set of participant coefficients $a_{n'}$ as:

$$\begin{cases} v(\mathbf{y}) = \sum_{n'=0}^{N'} a_{n'} v_{n'}(\mathbf{y}), \mathbf{y} \in S \\ p(\mathbf{x}) = \sum_{n'=0}^{N'} a_{n'} p_{n'}(\mathbf{x}), \mathbf{x} \in \Omega \end{cases} \quad (6)$$

where $v_{n'=n^2+n+m+1} = q_n^m$ and $p_{n^2+m+1} = S_n^m$.

Eq. (6) is the basement of the MRS-based NAH but must be properly truncated. The subscription convention in Eq. (6) is convenient for the discretized linear operation. Obviously, the truncation number N' in Eq. (6) and N in Eq. (2) are related by

$N' = (N + 1)^2$. The truncation number is crucial to the pressure evaluation as well as the number and positions of microphone array required in the NAH.

Determination of the number of most efficient modes is converted to seeking the truncation number of radiation efficiency σ_n making the upper bound of the radiated sound power converge to a given tolerance. A relative error of the upper bounded radiated sound power caused by new added modes for degree N in Eq. (2) with respective to the one produced by existing modes for degree less than N is defined as:

$$\varepsilon_N = \frac{(2N + 1)\sigma_N(k\tilde{r})}{\sum_{n=0}^{N-1} (2n + 1)\sigma_n(k\tilde{r})} \quad (7)$$

where \tilde{r} is the equivalent radius of the vibrating structure. The equivalent radius is the description of the spherical source which has the same average radiated sound power per unit area as that of the vibrating structure or holograms. Since the radiated sound power from the equivalent source and the vibrating structure as well as the holograms should be same, the requirement of same average radiated sound power per unit area makes the equivalent radius satisfy

$$\tilde{r} = \sqrt{S/4\pi} \quad (8)$$

where S represents area of structure in the determination of equivalent radius \tilde{r} .

Fortunately, for a specific dimensionless value $k\tilde{r}$, the radiation efficiency $\sigma_{N > N_c}$ is a strictly decreasing function with respect to the degree N after a certain degree N_c which can be obtained by its closed-form expression. Radiation efficiency σ_N and the relative error ε_N for the dimensionless size $0.1 \leq k\tilde{r} \leq 10$ and the varying degree from 0 to 7 are presented in **Figure 2a** and **b**, respectively. It shows that σ_N is a monotonously decreasing function and clearly distinguishes from each degree for $k\tilde{r} < 2.0$. There is a plateau on which σ_N starts to overlap for $k\tilde{r} > 2.0$. It means that those degrees of modes contribute to the radiated sound power almost equally and no one can be neglected, which is verified by the relative errors in **Figure 2b**. Therefore, more degrees of modes are needed to make the radiated sound power converge for larger dimensionless value $k\tilde{r}$. The relative error ε_N presented in **Figure 2b** can be used as a reference to determine the degree of the most efficient modes for $0.1 \leq k\tilde{r} \leq 10$, or in other words the

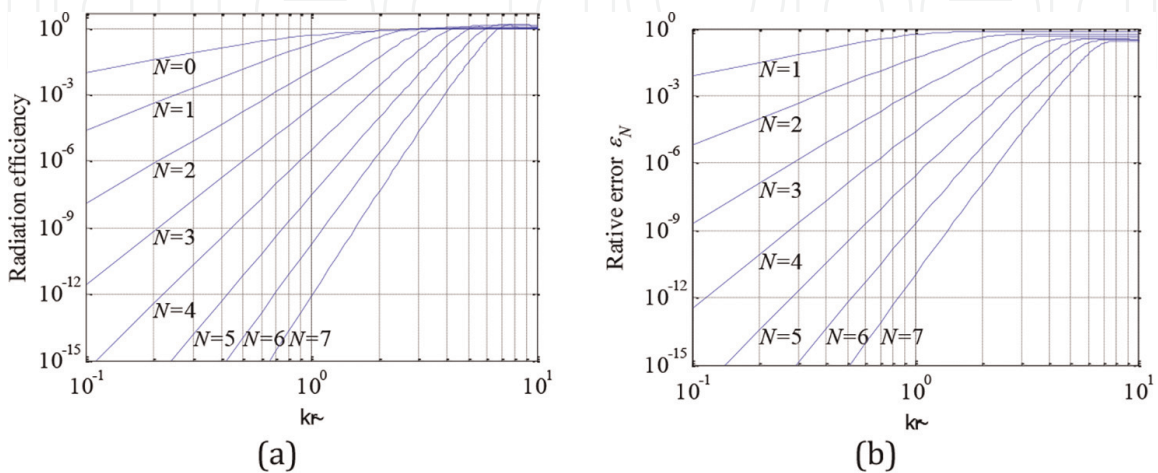


Figure 2. (a) Radiation efficiency of a sphere, and (b) relative errors of upper bounded radiated sound power, for varying degrees and $k\tilde{r}$.

truncation number N for the FS-based NAH. However, Eq. (7) only relates to the size of the structure and has nothing to do with the field point or size of hologram.

2.2 The NAH procedure

Suppose a set of at least independent velocity modes on the boundary, denoted as $v_i(\mathbf{x} \in S), (i = 1, 2, \dots)$, can produce a set of independent pressure modes $p_i(\mathbf{x} \in \Gamma), (i = 1, 2, \dots)$ on the measurement surface Γ , correspondingly, and they form a pair of bijective mapping relationship.

Generally, the pressure patterns $p_i(\mathbf{x} \in \Gamma)$ are non-orthogonal on the hologram, and an orthogonalization process is required, which can be done by the Gram-Schmidt approach as:

$$u_i(\mathbf{x}) = p_i(\mathbf{x}) - \sum_{j=1}^{i-1} \frac{\langle p_i(\mathbf{x}), u_j(\mathbf{x}) \rangle}{\|u_j(\mathbf{x})\|} u_j(\mathbf{x}) \quad (9)$$

where the inner product $\langle p, u \rangle = \int_{\Gamma} p(\mathbf{x}) u^*(\mathbf{x}) d\Gamma(\mathbf{x})$ and the norm $\|u\| = \sqrt{\langle u, u \rangle}$. After some algebraic operations, the normalized orthogonal modes $e_i(\mathbf{x}) = u_i(\mathbf{x}) / \|u_i(\mathbf{x})\|$ can be expressed in the following form:

$$\mathbf{E} = \mathbf{pR} \quad (10)$$

where $\mathbf{E} = [e_1(\mathbf{x}), e_2(\mathbf{x}), \dots]$, $\mathbf{p} = [p_1(\mathbf{x}), p_2(\mathbf{x}), \dots]$ and \mathbf{R} is a real upper triangular square matrix. As indicated in Eq. (10), the normalized orthogonal modes are actually a linear combination of the independent pressure modes p_i . It is remarkable that evaluation of the inner product is performed on holograms which are generally in smooth shapes, such as the three typical holograms in Section 0. Thus, they can be computed on exact geometries which are a void of discretization errors. Furthermore, orthogonalization of the modes on simple shaped holograms will yield a translation matrix \mathbf{R} with good numerical characteristics, such as the condition number.

Assume the radiated pressure $p(\mathbf{x})$ is decomposed into the normalized orthogonal modes $e_i(\mathbf{x})$ on the hologram as:

$$p(\mathbf{x}) = \sum_{i=1}^{\infty} \alpha_i e_i(\mathbf{x}) \quad (11)$$

where

$$\alpha_i = \langle p(\mathbf{x}), e_i(\mathbf{x}) \rangle_{\Gamma} \quad (12)$$

Once those participant coefficients are obtained by the measured pressure, substituting Eq. (10) into Eq. (12) yields

$$p(\mathbf{x}) = \sum_{i=1}^{\infty} \lambda_i p_i(\mathbf{x}) \quad (13)$$

where the coefficients are

$$\lambda_i = \sum_{j=i}^{\infty} R_{ij} \alpha_j \quad (14)$$

Due to the unique mapping relationship between surfaces of vibrating structure and hologram, reconstruction for the boundary quantities can be performed by multiplying the corresponding modes with the same set of participant coefficients λ_i on the surface of the vibrating structure.

Thus, acoustic holography is converted to seek explicit descriptions of the mapping relationship between the modes on the boundary and modes on the field and design a proper experimental setup for obtaining the participant coefficients of the modes on the measurement surface. The modes on the boundary are free of restrictions for their form of expression, which could be in any well-studied analytical functions or in generally numerical representations. However, it should be expected to have a capacity of fast convergent ratio in the decomposing of boundary quantities and generate a radiated pressure on the hologram which is easy to be determined by the experiment. In the current work, the FS in spherical coordinates for the Helmholtz equation Eq. (2) and its normal gradient Eq. (5) are chosen as the pressure and velocity modes. Merits of choosing those forms of modes are twofold. First, the radiated modes on the field are also the in the same form; and second, the most effective modes contributing to the field pressure are easy to be determined. Henceforth, the radiated pressure modes in Eq. (13) are chosen as $p_i = p_{n^2+m+n+1} = S_n^m$ in our analysis to facilitate derivations. So do the velocity modes q_i .

2.3 Setup of the microphone array

Since the modes are distributed on an enclosing surface, the holograms should form an enveloping surface enclosing the vibrating structure. Otherwise, partially measured pressure cannot represent the modes completely and consequently cannot be applied to reconstruct the boundary information based on the mapping relationship.

The distribution of a specific mode varies on different holograms. Generally, the measurements are subject to the experimental resource such as microphones and permissible space. How to accurately recognize the field pressure modes is one of the crucial factors to NAH. In practice, microphones are preferred to be placed on planar, cylindrical, or spherical surfaces which are easy to be set up but generally not conformal to the vibrating structure, as shown in **Figure 3**.

For the enclosing planar holograms, as shown in **Figure 3a**, each pressure mode is divided and projected onto six patches. On each patch, the measured pressure should be able to accurately represent the projected pressure modes. However, once the pressure is discretely sampled, the spectrum or the number of participant modes on

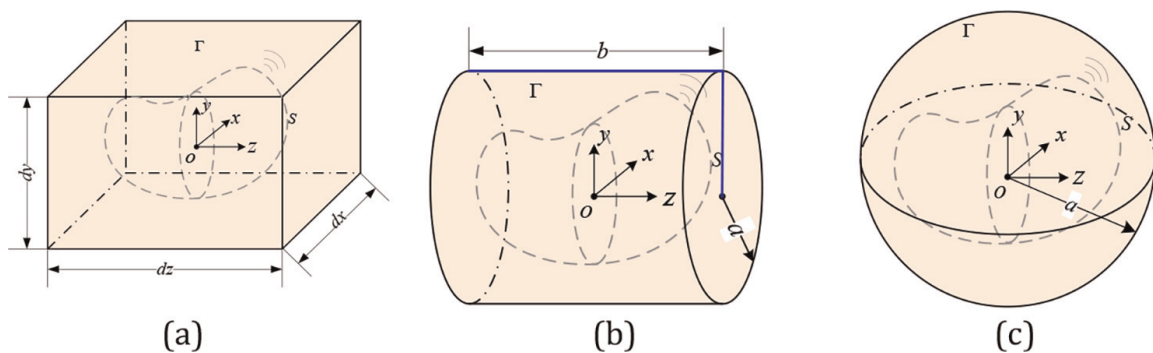


Figure 3. Three typical holograms: (a) planar holograms, (b) cylindrical holograms, and (c) spherical holograms.

that patch is truncated. Therefore, the primary task in the measurement is to set up the microphone arrays properly with an aim to approximate all the projected pressure modes on each patch actually. On each planar surface, the pressure modes can be expressed by two sets of locally orthogonal polynomials such as polynomial $f_n(x)$ and $g_m(y)$ of degree n and m in each direction, respectively. The most significant degrees in each direction can be numerically obtained directly by approximating the analytical pressure mode, Eq. (2), with the polynomial expansions $f_n g_m$, as

$$S_n^m(k, \mathbf{x}) = \sum_{n'=0}^{N'} \sum_{m'=0}^{M'} a_{n'}^{m'} f_{n'}(x(\mathbf{x})) g_{m'}(y(\mathbf{x})) \quad (15)$$

where $a_{n'}^{m'}$ is the coefficients. Once the polynomial degrees N' and M' on each planar patch are determined, the microphones are placed at the abscissas of Gaussian quadrature points on the patch, which results in $(N' + 1) \times (M' + 1)$ microphone positions [33].

A closed cylindrical measurement surface, as shown in **Figure 3b**, has three patches, one left circular planar patch $\Gamma_l(\mathbf{x} | b/2 = \|\mathbf{x}\| \cos \theta)$, one right $\Gamma_r(\mathbf{x} | b/2 = \|\mathbf{x}\| \cos \theta)$ circular planar patch, and one cylindrical surface $\Gamma_c(\mathbf{x} | a = \|\mathbf{x}\| \sin \theta)$ in the central portion. Similar to the planar hologram, it needs to select a set of locally orthogonal patterns to approximate the pressure modes on each patch. In this case, arguments θ and ϕ in cylindrical coordinates are the two independent variables to define patches. All three patches possess a complete description for the variable ϕ in the range $[0, 2\pi]$. In light of the expression for pressure modes, Eq. (2), normalized basis $g_m(\phi(\mathbf{x})) = e^{im\phi(\mathbf{x})} / \sqrt{2\pi}$ is selected as one set of the orthogonal patterns in the ϕ direction. Thus, the determination of the truncation number for another set of local basis function $f_{n'}$ is simplified to approximate the following function $\mathcal{F}_n(k, \mathbf{x}) = h_n(k\|\mathbf{x}\|) P_n^m(\cos \theta)$.

A spherical measurement surface is shown in **Figure 3c**, which is a conformal patch to the spherical coordinates upon which the FS is obtained. Field modes on the spherical surface are orthogonal. Determination of the field modes on the spherical hologram is actually to identify the spherical harmonic functions based on the measured pressure. Due to conformality of the hologram to the coordinate system of the spherical FS, an analytical way is available to determine the number and position of the measurement. The quadrature technique on a sphere is well studied and widely used in the computational acoustics [34]. Therefore, the participant coefficients in Eq. (12) can be accurately evaluated by $(N + 1)$ point Gaussian quadrature and $(2N + 1)$ point square quadrature for variables of θ and ϕ on the spherical surface for the pressure mode $S_N^m(|m| \leq N)$. Thus, it is free of numerical searching in the determination of the truncation number. In addition, the total number of measurements is the smallest than that requested by the other two holograms.

3. Error analysis

3.1 Error bounds on pressure energy

The NAH is an inverse problem and thus poses significant challenges to the stable and accurate solution. However, a practical measurement is prone to errors and always incorporates uncertainties, such as random fluctuations, effect of rapid decay

of the evanescent waves. Generally, the great affection to the reconstruction by the inevitable measurement errors is largely due to over-selected number of the basis (either in numerical or analytical form) which results in an ill-posed inverse operator. Fortunately, the number of basis or modes can be well estimated by an analytical way as introduced in Section 2. Thus, a pre-regularization process is embedded in the MRS-based NAH.

On the holograms, the error included pressure is simply modeled as:

$$p(\mathbf{x}) = p_0(\mathbf{x}) + n(\mathbf{x}), \text{ or } \mathbf{P} = \mathbf{P}_0 + \mathbf{n} \quad (16)$$

where \mathbf{P}_0 represents the source pressure and \mathbf{n} is the noise terms. Denote the signal-to-noise ratio (SNR) on the hologram as:

$$\text{SNR} = 10 \log_{10} \frac{W_{P_0}}{W_{Noise}} = 10 \log_{10} \frac{\int_{S_h} |P_0(\mathbf{x})|^2 dS(\mathbf{x})}{\int_{S_h} |n(\mathbf{x})|^2 dS(\mathbf{x})} \quad (17)$$

where W_{P_0} and W_{Noise} represent energies of source pressure and noise pressure, respectively. Under the condition that the source pressure and noise pressure can be completely decomposed by a set of modes, the SNR can be reformatted by the Parseval law as:

$$\text{SNR} = 10 \log_{10} \frac{\|\alpha_0\|_2^2}{\|\alpha_{Noise}\|_2^2} \quad (18)$$

where α_0 and α_{Noise} are coefficients of the locally normalized orthogonal patterns on the holograms for the source pressure and noise term, and correspondingly the coefficients for pressure \mathbf{P} is $\alpha = \alpha_0 + \alpha_{Noise}$.

By taking advantages of the mapping relationships, Eq. (11) is used to evaluate the reconstructed pressure on the surface of vibrating structure after the coefficients λ of FS are obtained on the holograms. Decompose the FS in Eq. (11) on the surface of vibrating structure as same as that in Eq. (10) but with symbol \mathbf{S} substituting for pressure mode \mathbf{p} as:

$$\mathbf{S}_\Gamma = \mathbf{E}_\Gamma \mathbf{R}_\Gamma^- \quad (19)$$

where \mathbf{E}_Γ is the column normalized modes on the surface of vibrating structure and \mathbf{R}_Γ is a translation operator which is an upper triangular square matrix. In light of Eq. (14) and Eq. (19), reconstructed sound pressure on surface of the vibrating structure, \mathbf{p}_Γ in the Eq. (13) can be expressed as:

$$\mathbf{p}_\Gamma = \mathbf{E}_\Gamma \mathbf{R}_\Gamma^- \mathbf{R} \alpha \quad (20)$$

Therefore, it could be observed that the reconstruction process is to translate the local coefficients α obtained on the holograms to that on the surface of vibrating structure by the translator $\mathbf{R}_\Gamma^- \mathbf{R}$, and then the reconstructed pressure is evaluated by the modal decomposition method. Stability of the translation is largely dependent on the product of the two translators \mathbf{R}_Γ^- and \mathbf{R} which are closely related to the geometric information of the structure and holograms, respectively.

According to the Parseval law, the reconstructed pressure energy on the surface of vibrating structure is

$$W_{P_\Gamma} = \|\mathbf{R}_\Gamma^- \mathbf{R} \boldsymbol{\alpha}\|_2^2 = \boldsymbol{\alpha}^* \mathbf{T}_R \boldsymbol{\alpha} \quad (21)$$

where $\mathbf{T}_R = \mathbf{R}^* \mathbf{R}_\Gamma^- \mathbf{R}_\Gamma^- \mathbf{R}$ is a Hermitian matrix. Therefore, there is an eigen decomposition of $\mathbf{T}_R = \mathbf{Q}^* \boldsymbol{\Lambda} \mathbf{Q}$ in which \mathbf{Q} is a unitary complex matrix whose columns comprise an orthonormal basis of eigenvectors of \mathbf{T}_R , and $\boldsymbol{\Lambda}$ is a real diagonal matrix whose main diagonal entries are the corresponding eigenvalues. Assume the eigenvalues are sorted in a descending order, such as $\Lambda_i \geq \Lambda_j$ for $j > i$. The lower and upper bounds of the reconstructed pressure energy are easy to be obtained

$$\Lambda_d \|\boldsymbol{\alpha}\|_2^2 \leq W_{P_\Gamma} \leq \Lambda_1 \|\boldsymbol{\alpha}\|_2^2 \quad (22)$$

where d is the dimension of the matrix. In practice, the relative error of reconstructed pressure energy on the surface of the vibrating structure is more concerned. Obviously, the bounds of the exact pressure energies $W_{P_{0\Gamma}}$ and noise generated pressure energies $W_{P_{noise\Gamma}}$ can be obtained with coefficients $\boldsymbol{\alpha}$ replaced with $\boldsymbol{\alpha}_0$ and $\boldsymbol{\alpha}_{Noise}$ in Eq. (22), respectively. Thus, bounds for the relative errors $\varepsilon_{W_\Gamma} = W_{P_{noise\Gamma}}/W_{P_{0\Gamma}}$ are

$$cond(\mathbf{T}_R)^{-1} 10^{-SNR/10} \leq \varepsilon_{W_\Gamma} \leq cond(\mathbf{T}_R) 10^{-SNR/10} \quad (23)$$

where $10^{-SNR/10} = \|\boldsymbol{\alpha}_{Noise}\|_2^2 / \|\boldsymbol{\alpha}_0\|_2^2$, and $cond(\mathbf{T}_R) = \Lambda_1/\Lambda_d$ is the condition number of the translator matrix \mathbf{T}_R . Eq. (23) can be reexpressed as:

$$SNR - \log_{10} cond(\mathbf{T}_R) \leq SNR_\Gamma \leq SNR + \log_{10} cond(\mathbf{T}_R) \quad (24)$$

in which $SNR_\Gamma = -\log_{10} \varepsilon_{W_\Gamma}$ is the signal-to-noise ratio of the reconstructed pressure on the model's surface.

3.2 The modified error bounds

Above analysis is based on an assumption that the pressure can be completely decomposed by a set of modes. Otherwise, the Parseval law cannot be applied equivalently in evaluating the pressure energy. However, the complete set of modes is hardly to be satisfied in decomposing the radiated pressure of a realistic radiator, but an incomplete set is applied to approximately decompose the radiated pressure within a given tolerance. Therefore, a compromise on accuracy and robustness is made by truncating the series expansion $N' = (N + 1)^2$, Eq. (6), with a proper number N such as that given by Eq. (7). Due to the truncation, the measured pressure energy evaluated by the modal decomposition method on holograms is not equal to the true quantities, and so is the noise energy. It is also reasonable to define SNR on the hologram by Eq. (18), because once the radiated pressure is spatially measured by limited number of microphones, such as the way introduced in Section 2.2, the higher frequency components are filtered out which will not go through the inverse system.

Suppose the exact pressure on the surface of the vibrating structure is $p_{0,\Gamma}$ and the corresponding reconstructed pressure is p_Γ . Therefore, the relative error of the reconstructed pressure energy in discretized form is

$$\varepsilon_{W_\Gamma} = \frac{\|\mathbf{P}_{0,\Gamma} - \mathbf{P}_\Gamma\|_2^2}{\|\mathbf{P}_{0,\Gamma}\|_2^2} \quad (25)$$

According to the derivation in the appendix in the ref. [35], the relative error ε_{W_Γ} can be expressed as:

$$\varepsilon_{W_\Gamma}(c_1, c_2, c_3, c_4) = \frac{c_4 + c_3 10^{-SNR/10} + c_1 \sqrt{c_4} \sqrt{c_3} 10^{-SNR/20}}{1 + c_4 + c_2 \sqrt{c_4}} \quad (26)$$

It reaches the lower bound at $c_1 = -2$ and $c_2 = 2$, and the upper bound at $c_1 = 2$ and $c_2 = -2$. However, Eq. (26) is a nonlinear function for variables c_3 , and constrained nonlinear optimization algorithm is sought to find the lower and upper bounds, as the minimum of a problem specified by:

$$\min_{(c_3)} f(c_3) \text{ such that } \text{cond}(\mathbf{T}_R)^- \leq c_3 \leq \text{cond}(\mathbf{T}_R) \quad (27)$$

where the objective function is

$$f(c_3) = \begin{cases} \varepsilon_{W_\Gamma}(-2, 2, c_3, c_4), & \text{for lower bound} \\ -\varepsilon_{W_\Gamma}(2, -2, c_3, c_4), & \text{for upper bound} \end{cases} \quad (28)$$

In the above analysis, the variables SNR and c_4 are supposed to be given. The SNR of the environment can be estimated by measurement. For the ideal cases in which there is no noise included, equivalent to $\text{SNR} = \infty$, the lower bound of the relative error is easy to be obtained as:

$$\varepsilon_{W_\Gamma} \geq \frac{c_4}{1 + c_4 + 2\sqrt{c_4}} \quad (29)$$

which is only related to the c_4 and in turn related to the number of adopted participant modes. The actual reconstructed error of a realistic problem or the case with small SNR are not expected to have a lower bound less than that estimated for no noise included case. Thus, the lower bound of the reconstructed pressure energy can be estimated by Eq. (29).

The variables c_4 is a crucial parameter for the error bounds estimation, which can either be evaluated by numerical simulation for specific problems or estimated by an analysis method. However, numerical simulation is hard to be realized for practical problems, since the source is not clear and it is the reason why the NAH is needed. Therefore, it is demand for developing a general analysis approach to properly estimate the variable c_4 . Whereas, it is out of our mathematical ability as well as the range of the current work. In the following numerical examples, variable c_4 is estimated by the numerical method, a combination of finite element method (FEM) and BEM.

3.3 Characteristics of the translator

To investigate how much the output value of a function, such as the reconstructed quantities, can change for a small variation, such as the errors introduced in the

experiment, in the input arguments, condition number of the function is one of the frequently used measure. Therefore, investigation of the condition number of translators in the NAH can somehow describe the stability of the reconstruction. Generally, numerical approach is applied to compute the condition number. However, if both shapes of the structure and holograms are conformal to sphere, a simple asymptotic expression of the condition number is available. The radii of spherical structure and holograms are denoted as r_Γ and r . Translators \mathbf{R}_Γ and \mathbf{R} are all diagonal matrices, taking the \mathbf{R} as an example:

$$\mathbf{R} = \text{diag} \left\{ \bigcup_{n=0}^N \left[\overbrace{|rh_n(kr)|^{-1} \cdots |rh_n(kr)|^{-1}}^{2n+1} \right] \right\} \quad (30)$$

where $\text{diag}\{\mathbf{v}\}$ means a square diagonal matrix with the elements of vector \mathbf{v} on the main diagonal, and $\bigcup_{n=0}^N \mathbf{v}_n$ returns a vector combining all the subvector \mathbf{v}_n . Thus,

$$\mathbf{T}_R = \text{diag} \left\{ \bigcup_{n=0}^N \left[\overbrace{\frac{|r_\Gamma h_n(kr_\Gamma)|^2}{|rh_n(kr)|^2} \cdots \frac{|r_\Gamma h_n(kr_\Gamma)|^2}{|rh_n(kr)|^2}}^{2n+1} \right] \right\} \quad (31)$$

According to the analysis in Ref. [36], the asymptotic expression of $|xh_n(x)|$ for $n \gg x$ is

$$|xh_n(x)| \sim \sqrt{\frac{2}{e}} \left(\frac{2l+1}{e} \right)^l x^{-n} e^{x^2/4n} \quad (32)$$

which is actually the absolute value of the imagine part of the spherical Hankel function, since the real part goes rapidly to zero for $n \gg x$; therefore,

$$\text{cond}(\mathbf{T}_R) = \frac{|r_\Gamma h_N(kr_\Gamma)|^2}{|rh_N(kr)|^2} \sim \left(\frac{r}{r_\Gamma} \right)^{2N} e^{k^2(r_\Gamma^2 - r^2)/2N} \sim \left(\frac{r}{r_\Gamma} \right)^{2N} \quad (33)$$

due to that $e^{k^2(r_\Gamma^2 - r^2)/2N}$ approximate rapidly to one for $N \gg kr_\Gamma$ and $N \gg kr$.

To investigate how much the reconstructed coefficients and in turn the pressure can change for a small variation in the local coefficients α , condition number of the translator $\mathbf{R}_\Gamma^{-1} \mathbf{R}$ is the quantity needs to be studied. In light of the previous analysis, the condition number of the translation operator $\mathbf{R}_\Gamma^{-1} \mathbf{R}$ for spherical structure and holograms satisfies

$$\text{cond}(\mathbf{R}_\Gamma^{-1} \mathbf{R}) = \frac{|r_\Gamma h_N(kr_\Gamma)|}{|rh_N(kr)|} \sim \left(\frac{r}{r_\Gamma} \right)^N \quad (34)$$

Actually, the condition number of translator \mathbf{T}_R is a square power of that for the translator $\mathbf{R}_\Gamma^{-1} \mathbf{R}$, i.e. $\text{cond}(\mathbf{T}_R) = \text{cond}(\mathbf{R}_\Gamma^{-1} \mathbf{R})^2$. Eq. (34) indicates that the condition number has a geometric growth with N under the condition $N \gg kr_\Gamma$ and $N \gg kr$. Correspondingly, the larger condition number of the translator will obviously increase the sensibility to the inevitable errors introduced in the experiment. In addition, the

large ratio of r/r_Γ could also increase the condition number for a fixed degree N . It implies that the same distance of the measurement to a smaller size surface will result in a reconstruction which is more prone to be contaminated. The condition numbers of the translator $\mathbf{R}_\Gamma^{-1}\mathbf{R}$ for a spherical model with radius being 0.1 m and spherical holograms at frequency 601 Hz are given in **Figure 4**, which clearly validates the asymptotic form Eq. (34) to the exact one, for $N \gg kr_\Gamma$ and $N \gg kr$.

The asymptotic expression of the condition number of the translator $\mathbf{R}_\Gamma^{-1}\mathbf{R}$ for general models and holograms are hardly to be obtained. Numerical method is resorted to get the condition number once the frequency, geometrical information of the model as well as holograms are supplied. To explore the influence of shapes of the model and holograms to the condition number, case studies of a cubic model with planar holograms and spherical holograms, which are representatives as conformal measurement and non-conformal measurement, are performed. The cubic model is same as that used in the numerical examples in Section 4. The planar holograms and spherical hologram also have the same configuration as that in the numerical examples. Two frequencies 601 Hz and 1333 Hz are analyzed. The condition numbers obtained by numerical method and asymptotic are presented in **Figure 5**. It is noticeable that the asymptotic condition number of the cubic model with planar holograms are evaluated with their equivalent radii. It can be observed that the asymptotic expression for planar holograms, which is a conformal hologram to the model, approximates to that obtained numerically very well for the frequency 601 Hz. However, the approximation does not show up for the frequency 1333 Hz up to the degree $N = 10$. It is because that the larger dimensionless value $k\tilde{r}$ needs larger degree to satisfy the condition of the asymptotic expression. The asymptotic estimation of the condition number does not work well for the spherical holograms due to the disparity in shapes with the cubic model. Even the ratio r/\tilde{r}_Γ for the spherical hologram is smaller than that of the planar hologram, the condition number for the spherical hologram is inclined to be larger than that for the planar holograms as illustrated in **Figure 5**. It implicates that a cubic model with spherical hologram, a representative case of non-conformal measurement, may be more sensitive to measurement errors than that with planar hologram.

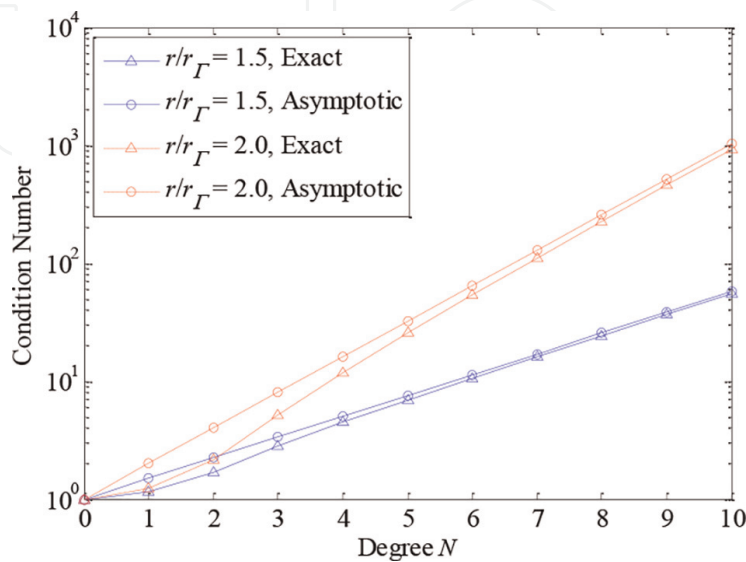


Figure 4. The exact and asymptotic condition numbers of the translator $\mathbf{R}_\Gamma^{-1}\mathbf{R}$ for different ratio r/r_Γ for spherical model and holograms.

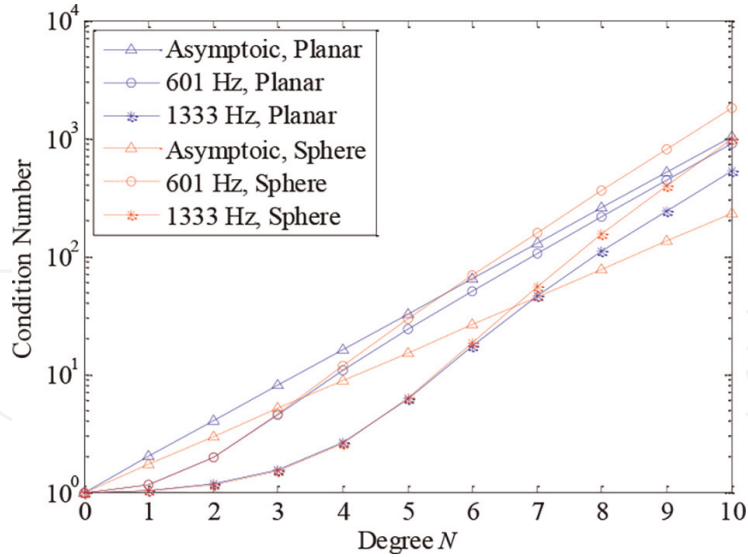


Figure 5. The asymptotic and numerical condition numbers of the translator $\mathbf{R}_T \mathbf{R}$ for a cubic model with planar holograms and spherical holograms at two frequencies.

4. Experiment study

4.1 Numerical simulation

The necessary number of participant modes is hard to be obtained exactly for a realistic problem, and truncation error is introduced. In this case, the radiated source pressure on holograms is generated from a vibrating cubic model driven by a harmonic excitation. As shown in **Figure 6**, the cubic model is of size $0.2\text{m} \times 0.2\text{m} \times 0.2\text{m}$ and is excited by a harmonic force along z-axial at a specified position $(0.4a, 0.4a, -0.5a)$, and the four corners at the bottom are constrained. Thicknesses of the six walls are set as 0.004 m , and the steel material is assigned to the model. The harmonic response is obtained by a commercial finite element software at frequencies 601 Hz , which is chosen closely to the one modal frequency with an aim to obtain a uniformly distributed velocity on the surface. Once the boundary velocities are obtained, the radiated sound pressure at the measurement positions are computed by the boundary element method [37] as the inputs for the reconstruction. It is to simulate the realistic radiator whose exact number of efficient modes is hardly to be obtained but estimated by a reasonable guideline. Both of the cases include a specific amount of noise with prescribed SNR on the hologram. The noise is generated with

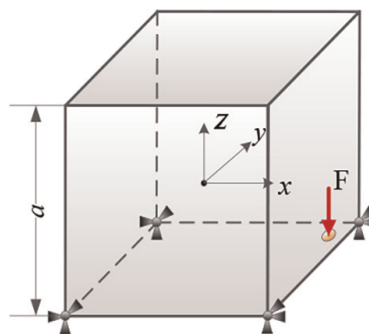


Figure 6. Configuration of the cubic model excited by harmonic force F (denoted by the red arrow) along the z-axis.

$$\mathbf{n} = \gamma \mathbf{S} \boldsymbol{\lambda}_{Noise} \quad (35)$$

where $\boldsymbol{\lambda}_{Noise}$ is a Gaussian random vector, and $\gamma = 10^{-SNR/20} \|\mathbf{R}^{-1} \boldsymbol{\lambda}_{Noise}\|_2^{-1} \sqrt{W_{P_0}}$ is an energy-related variable to make sure the generated noise \mathbf{n} can form a specified SNR.

In this section, investigations are devoted to the reconstructions of the NAH with spherical holograms. To use the MRS-based NAH, the primary task is to determine the number of necessary modes. According to the method introduced in Section 2.1, the equivalent radius of the cubic model is $\tilde{r} = \sqrt{3/2\pi a}$ which results in dimensionless variables $k\tilde{r}$ equal to 1.53. The energy criteria Eq. (7) are adopted to determine the necessary number of FS due to its reasonable compromise on the accuracy and efficiency in the reconstruction. The tolerance is set as $\varepsilon_T = 1E-1$, and it yields the necessary number of FS being 3 by referring to the diagram in **Figure 2**. The number and position of microphones are consequently determined by the approach in Section 2.3. To investigate the influence of the necessary number to the final results, reconstructions are performed for the necessary number ranging from 3 to 6 for each case.

There are errors due to the truncation of the participant modes. Therefore, reconstructions are firstly performed for the pressure \mathbf{p}_{num} obtained numerically by the FEM and BEM which are also treated as the exact source pressures. The reconstructions are considered as the references of no-noise included measurement. Contour plots of the reconstructed pressure for reference cases are given in **Figure 7**. In spite of a slight disparity in the quantity, it can be observed that the reference reconstructions are very satisfied with the simulated pressure, because the significant pressure distributions are well reconstructed. Later on, different SNRs ranging from 4 dB to 28 dB with the increment being 4 dB are added to the simulated pressure to validate the robustness of the NAH to the noise which is unavoidable in the realistic experiment. The noise is obtained by Eq. (35).

Relative errors of reconstructed pressure energy on the model's surface is defined as:

$$\varepsilon_{W_r} = \frac{\|\mathbf{p}_{recon} - \mathbf{p}_{num}\|_2^2}{\|\mathbf{p}_{num}\|_2^2} \quad (36)$$

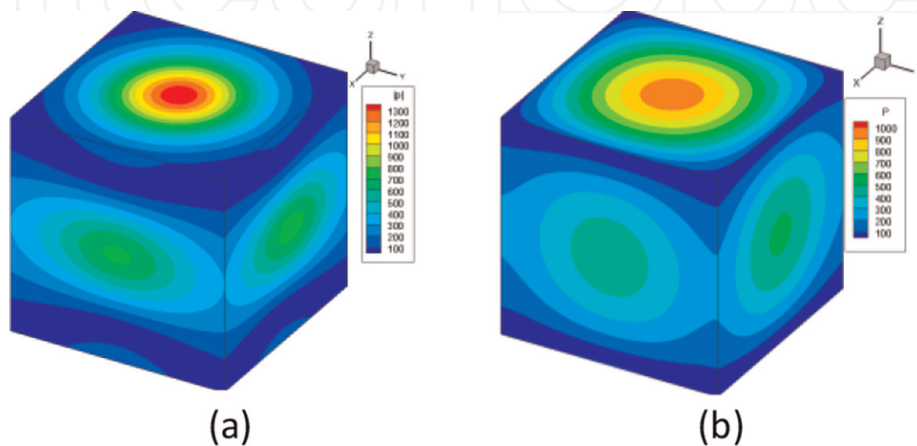


Figure 7. The reconstructed pressure on the boundary based on the no-noised included measurement on (a) the spherical holograms with the necessary number of modes $N = 3$ for (b) the simulated results at frequency 601 Hz.

where \mathbf{p}_{recon} is the reconstructed pressure based on different SNRs. To estimate the error, variable c_4 is required to be supplied by:

$$c_4 = \frac{\|\mathbf{p}_{recon}\|_2^2}{\|\mathbf{p}_{recon} - \mathbf{p}_{num}\|_2^2} \quad (37)$$

based on the simulated results. According to bounds Eq. (26), normalized relative errors of pressure energy are defined as:

$$\tilde{\epsilon}_{W_r} = \frac{(10^{SNR/10} \epsilon_{W_r} - \text{cond}(\mathbf{T}_R)^-)}{\text{cond}(\mathbf{T}_R) - \text{cond}(\mathbf{T}_R)^-} \quad (38)$$

for different SNRs and holograms, which should satisfy $\tilde{\epsilon}_{W_r} \in [0, 1]$.

The errors are plotted in **Figure 8**. **Figure 8a** depict that the most necessary number of modes for the boundary pressure reconstruction is $N = 3$. However, the reconstruction with $N = 4$ is superior to that of $N = 5$ in the sense of stability. Because the condition numbers of translators for $N = 5$ are larger which results in an inverse operation sensitive to errors. Actually, condition number for $N = 5$ is more than six times of that for $N = 4$ which reduces the reconstruction accuracy by the amplified errors. It is also the reason why the results obtained with $N = 5$ is worse than $N = 4$ for SNRs smaller than 20 dB even that it has a smaller radiation efficiency error in **Figure 2**. The decreased results for the reconstructed pressure with increased number of necessary modes illustrate that over-selected number of modes may result in accuracy loss, especially for models with irregular shapes as well as small SNRs. It is because that over-selected number of modes will yield translators with larger condition numbers which are likely to amplify the errors in the reconstruction. It is also observed from **Figure 8** that the two types of holograms can deliver the same level of accuracy with proper selected number of modes. However, the spherical hologram is more preferable since it requires the smallest number of microphones as compared with others.

The normalized errors are presented in of **Figure 8b**. The normalized errors are all less than 1 and increase along with the SNRs. The small errors for small SNRs and participant number of modes are due to the fact their lower bounds are

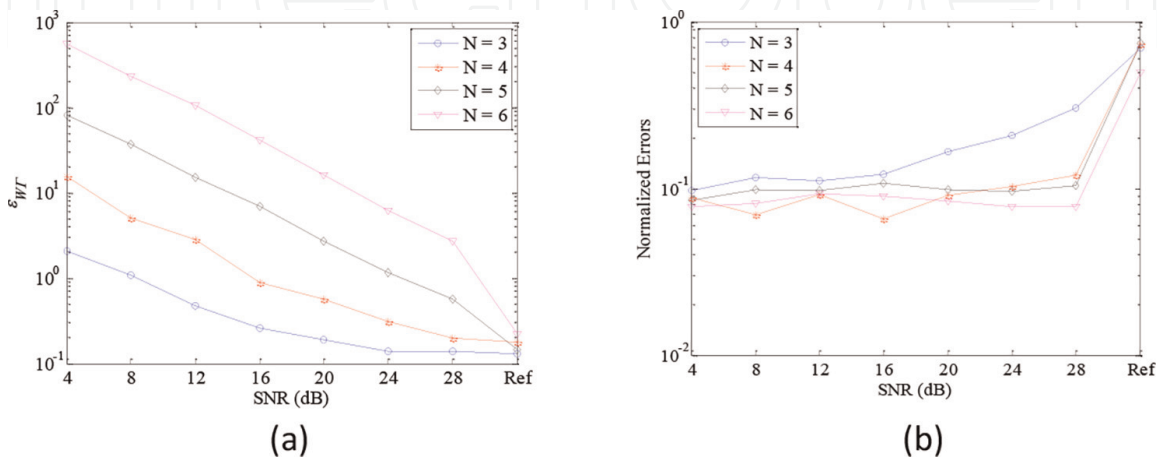


Figure 8. Errors of the reconstructed pressure energy with spherical holograms at 601 Hz for (a) the relative error ϵ_{W_r} and (b) the normalized error $\tilde{\epsilon}_{W_r}$.

underestimated, while the upper bounds are overestimated by the approach in Section 3.3. The extreme small normalized errors for case $N = 3$ are due to the dominated truncation errors for small number of adopted participant modes. As indicated for the reference cases, also the no-noise included cases, the reconstructed errors are closer to 1, or in other words more approximated to the estimated upper bounds. More important than the cases with small SNRs for which the estimated lower bounds are almost 0, the no-noise included cases (with infinity large SNR) can supply more reasonable lower bounds by the approach in Section 3.3. The numerical examples clearly demonstrated the validity of the proposed bounds estimation.

4.2 A practical experiment

An experiment is set up to explore the performance of the MRS-based NAH in this section. The source is in the same size and possesses the same material property as the one in the Section 4.1. Reconstruction is only preformed on the spherical hologram, since it requires the minimum number of microphones by comparing with the other two types of holograms.

An equipment is designed to facilitate the measurement. As shown in **Figure 9a**, the measurement on a spherical hologram is realized by rotating a half circular album arm, on which the microphones are mounted, around an axial which is the z-axis. The cubic model is placed at the center of the spherical hologram by hanging in a portal frame with a rigid hollow rod. A single-point drive is applied to the model by a small exciter on the top surface, as shown in **Figure 9b**. To make sure a uniform velocity distribution is generated on the surface, the analyzing frequency is selected closely to one of modal frequencies, which is 634 Hz. The model has an equivalent radius $\tilde{r} = 0.138\text{m}$, and the measurements are performed on a spherical hologram apart from the equivalent sphere by $\Delta = 0.1\text{ m}$. In light of Eq. (13), the necessary degree of the FS is adopted as $N = 3$. Correspondingly, the minimum required microphones along the θ and ϕ direction are 4 and 7, respectively. Here, we made an oversampling by placing five microphones along the θ direction and taking nine sequential measurements along ϕ direction

To validate the reconstructed results, the same 5 by 9 measurements are performed on a spherical validation surface Ω with radius being 0.18 m. In light of Eq. (13), the

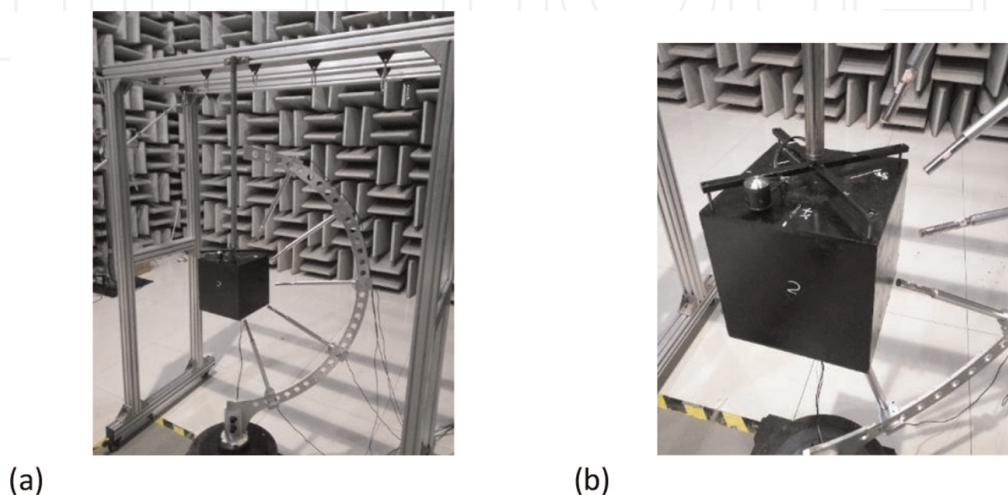


Figure 9.
The experimental setup: (a) overview of the configuration and (b) details of the model.

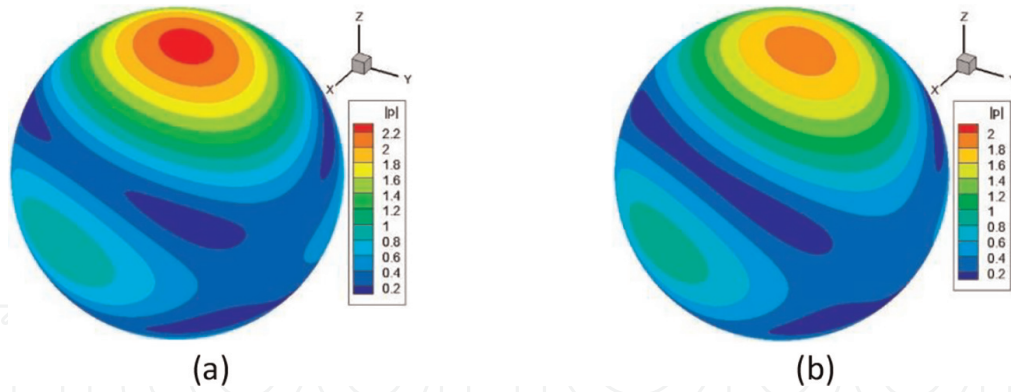


Figure 10.

The radiated pressure distribution on a spherical validation surface for (a) reconstructed from the hologram and (b) obtained from the direct measurement.

relative difference of reconstructed pressure with respect to the measured one on the validation surface is denoted by:

$$\varepsilon_{W_\Omega} = \frac{\left\| \sum_{n=0}^{(N+1)^2} (\lambda_n - \lambda_{n,\Omega}) p_n(k, \mathbf{x}) \right\|_2}{\left\| \sum_{n=0}^{(N+1)^2} \lambda_{n,\Omega} p_n(k, \mathbf{x}) \right\|_2} \quad (39)$$

where λ_n and $\lambda_{n,\Omega}$ are coefficients obtained on the hologram and validation surfaces, respectively. **Figure 10** depicts a comparison of the radiated pressure distribution on a spherical surface between the one reconstructed from the hologram and the one measured directly on the validation surface. It is clearly observed that the reconstructed pressure has a very satisfactory distribution agreement with the measured one for which the ε_{W_Ω} is 4.5% and the relative error of the maximum pressure is 21.8%.

The experiment is done in a semi-anechoic chamber which can reduce the influences of the environmental noise. Even that, positional errors and some other uncertainties are inevitable to be included in the measured signals which in turn affects the reconstruction results. The error analysis in Section 3 ascribes them to the SNR. How those relate to the SNR is crucial to the error estimation, which needs more investigation.

5. Conclusions

A NAH based on the mapping relationship between modes on surfaces of structure and hologram is introduced. The modes adopted in the NAH are FS of the Helmholtz equation in spherical coordinates which are generally independent and not orthogonal except on the spherical surface. The NAH framework provides a new insight to the reconstruction procedure based on the FS in spherical coordinates. The modes on the surface of structure and hologram form a bijective mapping. Number of modes prescribed in the MRS-based NAH is crucial to total number of measurement as well as the final reconstruction accuracy. An approach is proposed to estimate the necessary degree of effective modes. It is built on the energy criteria by exploring the radiation efficiency of the modes on the equivalent spherical source. An upper bounded error is derived for the radiated sound power of a vibrating structure with degree of modes up to a specific value. A relatively small value of degree is given by this approach.

Once the necessary degree of modes is determined, the number and position of microphones, which are also very crucial to the NAH, are investigated. Techniques to approximate the modes on three types of holograms by a set of locally orthogonal patterns are developed. A numerical algorithm is needed to determine the tight bounds for two locally orthogonal patterns on the planar patch. Due to the completeness of polar angles on cylindrical holograms, the algorithm is reduced by one dimension and the number of degree and positions are analytically determined for the local patterns along the polar direction. The number and position of measurement on the spherical hologram are determined by a purely analytical method because of its conformity to the coordinates of modes.

Errors are inevitable to be encountered in the NAH experiment. It is found that the reconstruction accuracy is subjected to two kinds of errors, one is the SNR and another one is the truncation error due to the limited number of participant modes adopted in the MRS-based NAH. An error model is built, and the relative error of the reconstructed pressure energy on the surface of the vibrating structure is derived. The lower and upper bounds of the relative error can be achieved numerically by a constrained nonlinear optimization algorithm. However, the approach generally yields underestimation of the lower bound and the overestimation of the upper bound, especially for MRS-NAH with large condition numbers. Alternatively, a reasonable lower bound is obtained by considering the case without noise or equivalently with positive infinite SNR. It eliminates the influence of the condition number of the inverse translator and is only related to the truncation errors. Thus, it is feasible to predicate the lower error of a reconstruction with the MRS-based NAH once the truncation error is given, which is validated by numerical examples. Proper estimation of the truncation errors is highly related to the reasonable estimation of the lower bound, which deserves more investigation.

Numerical examples are set up to validate the error analysis of the MRS-based NAH. It clearly demonstrates that the reconstructed results agree well with the simulated results. Physical experiment is designed to further demonstrate the feasibility and performance of the MRS-based NAH. The reconstructed results demonstrate a very satisfactory agreement with the direct measured one with respect to the quantities as well as the distribution on the validated surface. However, to estimate the performance with respect to the actual quantities by the proposed approach, it is desirable to investigate the influences of positional errors and other uncertainties on the SNR.

Acknowledgements

The work is supported by the National Natural Science Foundation of China (Grant No. 11404208).

Notes/thanks/other declarations

Place any other declarations, such as “Notes,” “Thanks,” etc. in before the References section. Assign the appropriate heading. Do NOT put your short biography in this section. It will be removed.

IntechOpen

Author details


Haijun Wu^{1,2*} and Weikang Jiang^{1,2}

1 State Key Laboratory of Mechanical System and Vibration, Shanghai Jiao Tong University, Shanghai, China

2 Institute of Vibration, Shock and Noise, Collaborative Innovation Center for Advanced Ship and Deep-Sea Exploration, Shanghai Jiao Tong University, Shanghai, China

*Address all correspondence to: haijun.wu@sjtu.edu.cn

IntechOpen

© 2022 The Author(s). Licensee IntechOpen. This chapter is distributed under the terms of the Creative Commons Attribution License (<http://creativecommons.org/licenses/by/3.0>), which permits unrestricted use, distribution, and reproduction in any medium, provided the original work is properly cited. 

References

- [1] Williams EG, Maynard JD, Skudrzyk E. Sound source reconstructions using a microphone array. *Journal of the Acoustical Society of America*. 1980;**68**(1):340-344
- [2] Maynard JD, Williams EG, Lee Y. Nearfield acoustic holography: I. theory of generalized holography and the development of NAH. *Journal of the Acoustical Society of America*. 1985; **78**(4):1395-1413
- [3] Veronesi WA, Maynard JD. Nearfield acoustic holography (NAH) II. Holographic reconstruction algorithms and computer implementation. *Journal of the Acoustical Society of America*. 1987;**81**(5):1307-1322
- [4] Williams EG. *Fourier Acoustics Sound Radiation and Nearfield Acoustical Holography*. San Diego, Calif: Academic Press; 1998
- [5] Steiner R, Hald J. Near-field acoustical holography without the errors and limitations caused by the use of spatial DFT. *International Journal of Acoustics and Vibration*. 2001;**6**(2): 83-8989
- [6] Cho YT, Bolton JS, Hald J. Source visualization by using statistically optimized near-field acoustical holography in cylindrical coordinates. *Journal of the Acoustical Society of America*. 2005;**118**(4):2355-2364
- [7] Hald J. Basic theory and properties of statistically optimized near-field acoustical holography. *Journal of the Acoustical Society of America*. 2009; **125**(4):2105-2120
- [8] Kim GT, Lee BH. 3-D sound source reconstruction and field reprediction using the Helmholtz integral equation. *Journal of Sound and Vibration*. 1990; **136**(2):245-261
- [9] Bai MR. Application of BEM (boundary element method)-based acoustic holography to radiation analysis of sound sources with arbitrarily shaped geometries. *Journal of the Acoustical Society of America*. 1992;**92**(1):533-549
- [10] Veronesi WA, Maynard JD. Digital holographic reconstruction of sources with arbitrarily shaped surfaces. *Journal of the Acoustical Society of America*. 1989;**85**(2):588-598
- [11] Zhang Z et al. A computational acoustic field reconstruction process based on an indirect boundary element formulation. *Journal of the Acoustical Society of America*. 2000;**108**(5 I): 2167-2178
- [12] Zhang Z et al. Source reconstruction process based on an indirect variational boundary element formulation. *Engineering Analysis with Boundary Elements*. 2001;**25**(2):93-114
- [13] Schuhmacher A et al. Sound source reconstruction using inverse boundary element calculations. *Journal of the Acoustical Society of America*. 2003; **113**(1):114-127
- [14] Johnson ME et al. An equivalent source technique for calculating the sound field inside an enclosure containing scattering objects. *Journal of the Acoustical Society of America*. 1998; **104**(3 I):1221-1231
- [15] Jeon IY, Ih JG. On the holographic reconstruction of vibroacoustic fields using equivalent sources and inverse boundary element method. *Journal of the Acoustical Society of America*. 2005; **118**(6):3473-3482

- [16] Sarkissian A. Method of superposition applied to patch near-field acoustic holography. *Journal of the Acoustical Society of America*. 2005; **118**(2):671-678
- [17] Bi CX et al. Nearfield acoustic holography based on the equivalent source method. *Science in China, Series E: Technological Sciences*. 2005; **48**(3): 338-353
- [18] Bi CX, Chen XZ, Chen J. Sound field separation technique based on equivalent source method and its application in nearfield acoustic holography. *Journal of the Acoustical Society of America*. 2008; **123**(3): 1472-1478
- [19] Bi CX, Bolton JS. An equivalent source technique for recovering the free sound field in a noisy environment. *Journal of the Acoustical Society of America*. 2012; **131**(2):1260-1270
- [20] Song L, Koopmann GH, Fahnlne JB. Numerical errors associated with the method of superposition for computing acoustic fields. *Journal of the Acoustical Society of America*. 1991; **89**(6): 2625-2633
- [21] Fahnlne JB, Koopmann GH. A numerical solution for the general radiation problem based on the combined methods of superposition and singular-value decomposition. *Journal of the Acoustical Society of America*. 1991; **90**(5):2808-2819
- [22] Koopmann GH, Song L, Fahnlne JB. A method for computing acoustic fields based on the principle of wave superposition. *Journal of the Acoustical Society of America*. 1989; **86**(6): 2433-2438
- [23] Bai MR, Chen CC, Lin JH. On optimal retreat distance for the equivalent source method-based nearfield acoustical holography. *Journal of the Acoustical Society of America*. 2011; **129**(3):1407-1416
- [24] Wu SF. On reconstruction of acoustic pressure fields using the Helmholtz equation least squares method. *Journal of the Acoustical Society of America*. 2000; **107**(5 I): 2511-2522
- [25] Wang Z, Wu SF. Helmholtz equation-least-squares method for reconstructing the acoustic pressure field. *Journal of the Acoustical Society of America*. 1997; **102**(4):2020-2032
- [26] Wu SF, Yu JY. Reconstructing interior acoustic pressure fields via Helmholtz equation least-squares method. *Journal of the Acoustical Society of America*. 1998; **104**(4):2054-2060
- [27] Wu SF. Methods for reconstructing acoustic quantities based on acoustic pressure measurements. *Journal of the Acoustical Society of America*. 2008; **124**(5):2680-2697
- [28] Thite AN, Thompson DJ. The quantification of structure-borne transmission paths by inverse methods. Part 1: Improved singular value rejection methods. *Journal of Sound and Vibration*. 2003; **264**(2):411-431
- [29] Williams EG. Regularization methods for near-field acoustical holography. *Journal of the Acoustical Society of America*. 2001; **110**(4): 1976-1988
- [30] Lu HC, Wu SF. Reconstruction of vibroacoustic responses of a highly nonspherical structure using Helmholtz equation least-squares method. *Journal of the Acoustical Society of America*. 2009; **125**(3):1538-1548

- [31] Bi CX et al. Reconstruction of the free-field radiation from a vibrating structure based on measurements in a noisy environment. *Journal of the Acoustical Society of America*. 2013; **134**(4):2823-2832
- [32] Abramowitz M, Stegun IA. *Handbook of Mathematical Functions with Formulas, Graphs, and Mathematical Tables*. Washington: U.S. Govt. Print. Off; 1964
- [33] Wu HJ, Jiang WK, Zhang HB. A mapping relationship based near-field acoustic holography with spherical fundamental solutions for Helmholtz equation. *Journal of Sound and Vibration*. 2016;**373**(7):66-88
- [34] Wu HJ, Liu YL, Jiang WK. A fast multipole boundary element method for 3D multi-domain acoustic scattering problems based on the Burton-miller formulation. *Engineering Analysis with Boundary Elements*. 2012;**36**(5):779-788
- [35] Wu HJ, Jiang WK. Experimental study of the mapping relationship based near-field acoustic holography with spherical fundamental solutions. *Journal of Sound and Vibration*. 2017;**394**: 185-202
- [36] Rahola J. Diagonal forms of the translation operators in the fast multipole algorithm for scattering problems. *BIT Numerical Mathematics*. 1996;**36**(2):333-358
- [37] Wu HJ, Liu YJ, Jiang WK. A low-frequency fast multipole boundary element method based on analytical integration of the hypersingular integral for 3D acoustic problems. *Engineering Analysis with Boundary Elements*. 2013; **37**(2):309-318